Alcohol oxidase protein mediated *in-situ* synthesized and stabilized gold nanoparticles for developing amperometric alcohol biosensor

Somasekhar R. Chinnadayyala, Mallesh Santhosh, Naveen K. Singh, Pranab Goswami

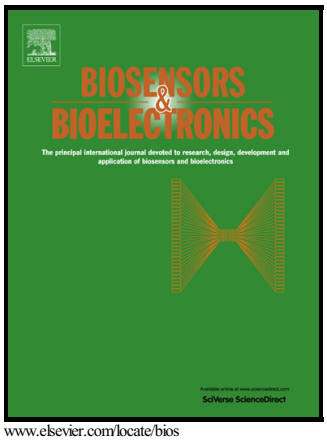

www.elsevier.com/locate/bios

PII: S0956-5663(15)00106-2
DOI: http://dx.doi.org/10.1016/j.bios.2015.02.015
Reference: BIOS7464

To appear in: *Biosensors and Bioelectronic*

Received date: 23 December 2014
Accepted date: 9 February 2015

Cite this article as: Somasekhar R. Chinnadayyala, Mallesh Santhosh, Naveen K. Singh and Pranab Goswami, Alcohol oxidase protein mediated *in-situ* synthesized and stabilized gold nanoparticles for developing amperometric alcohol biosensor, *Biosensors and Bioelectronic,* http://dx.doi.org/10.1016/j.bios.2015.02.015

Alcohol oxidase protein mediated *in-situ* synthesized and stabilized gold nanoparticles for developing amperometric alcohol biosensor.

Somasekhar R. Chinnadayyala, Mallesh Santhosh, Naveen K. Singh, Pranab Goswami*

Department of Biotechnology, Indian Institute of Technology Guwahati, Guwahati 781039, Assam, India

Running title: Alcohol oxidase protein mediated synthesis of gold nanoparticles

***Correspondence:** Fax: +91 361 2582249; Tel: +91 361 2582202; E-mail: pgoswami@iitg.ernet.in (P. Goswami)

Abstract

A simple one step method for the alcohol oxidases (AOx) protein mediated synthesis of gold nano particles (AuNPs) in alkaline (pH 8.5) condition with simultaneous stabilization of the nanoparticles on the AOx protein surface under native environment has been developed. The formation of the AOx conjugated AuNPs was confirmed by advanced analytical and spectroscopic techniques. The significant increase in zeta potential (ζ) value of -57 mV for the synthesised AOx-AuNPs conjugate from the AOx (p*I* 4.5) protein (ζ, -30 mV) implied good stability of the *in-situ* synthesised nano-conjugate. The AOx-AuNPs conjugate showed steady stability in alkaline (upto pH 8.5) and NaCl (up to10^{-1} M) solutions. The efficiency (K_{cat}/K_m) of the AuNP conjugated AOx was increased by 18 % from the free enzyme confirming the activating role of the surface stabilized AuNPs for the enzyme. The AuNPs–AOx conjugate was encapsulated with polyaniline (PANI) synthesised by oxidative polymerization of aniline using H_2O_2 generated *in-situ* from the AOx catalysed oxidation of alcohol. The PANI encapsulated AuNPs–AOx assembly was stabilized on a glassy carbon electrode (GCE) by chitosan–nafion mixture and then utilized the fabricated bioelectrode for detection of alcohol amperometrically using H_2O_2 as redox indicator at +0.6 V. The constructed biosensor showed high operational stability (6.3 % loss after 25 measurements), wide linear detection range of 10 μM – 4.7 mM (R^2= 0.9731), high sensitivity of 68.3±0.35 μA mM^{-1} and low detection limit of 7±0.027 μM for ethanol. The fabricated bioelectrode was successfully used for the selective determination of alcohol in beverage samples.

Key words: Alcohol oxidase; Gold nanoparticles; Polyaniline; Alcohol Biosensor; Hydrogen peroxide; Amperometry.

Introduction

Gold nanoparticles (AuNPs) have drawn remarkable research interest from the past decade owing to their potential applications in developing biosensors and in many other areas of technological front (Syed, 2014; Omidfar et al., 2013; Prakash et al., 2013; Huang et al., 2013). The wide utility of these nanoparticles has prompted to explore different synthesis routes that fit well with their intended applications. Focus has recently been laid on the green synthesis route for their production using a variety of biological materials, though the synthetic mechanism in most of the cases yet to be adequately explored (Zhong et al., 2004; Si and Mandal, 2007; Hussain et al., 2009; Shankar et al., 2005). Since the stability of the AuNPs formed in the reaction medium is an important criterion for their efficient collections and utilizations, hence studies on the application of various conditions and substances to prepare stable colloidal AuNPs have also received substantial research interest (Bajpai et al., 2007; Spirin et al., 2005; Rangnekar et al., 2007).

AuNPs have been widely studied for developing enzyme based electrochemical biosensors. The favourable functional traits of these nanoparticles that drive these studies are their strong electrical and biocompatible properties. The other reason of using AuNPs in amperometric biosensors is their high surface to volume ratio, which is a common property of the nanoparticles that serves to increase the enzyme loading on the electrode surface for amplifying the sensor signal and tailored wider detection range (Saxena et al., 2011). The coupling of AuNPs with the enzyme molecules is however, a critical issue to utilize the intended properties of the nanoparticles for achieving the desired level of response of the constructed biosensors. Moreover, the mode of coupling significantly influences the reproducible response characteristics of the constructed biosensors. For example, the high linker distance between the enzyme protein and AuNPs obtained by common chemical immobilization may interferes the electrocatalytic response of the biosensor, while the

physical immobilization may impair the stable interaction between the enzyme and the AuNPs thus hindering the reproducible performance of the constructed biosensors (Saxena and Goswami, 2012). An affable coupling for the desired functional properties may be difficult to achieve when the enzyme used is a labile protein such as AOx, which is a multimeric protein with Mw ~600 kDa. The study on AOx as biorecognition element for biosensors is increasingly growing due to its several advantages being recognised and among which the irreversible catalytic conversion of alcohols to carbonyl products and surpassing the need of supplementing co-factor to the reaction medium are prominent (Goswami et al., 2013; Azevedo et al., 2005). We report here AOx protein mediated *in-situ* synthesised and stabilized gold nanoparticles as activating and enhanced enzyme loading material for developing amperometric alcohol biosensor. In this approach the synthesis and stabilization of the NPs on the AOx protein surface were performed in single step by exploiting a spontaneous native reaction process driven by the enzyme protein itself under alkaline environment. We observed that the AOx molecules capping the nanoparticles retain their native structure to a reasonably good extent and were stable in high saline conditions. The AOx coupled AuNPs were encapsulated with polyaniline (PANI) synthesised by oxidative polymerization of aniline using H_2O_2 generated *in-situ* from the AOx catalysed oxidation of alcohol. PANI offers a great advantage for immobilization of enzymes because of its biocompatibility, stability and controllable electrochemical properties (Zhao et al., 2009). The PANI/AOx-AuNPs composite was stably dispersed on the GCE by using chitosan (chit) and Nafion (Nf) through their excellent film forming abilities. Nafion polymer also acts as a selective barrier for the restricted access of many interferents to the electrode surface by electrostatic repulsion (Wang et al. 2003; Sarma et al., 2009), while chitosan is a biocompatible polymer and it supports freeze protection and prevent dissolution of the enzyme from the electrode surface due to its insoluble nature in neutral and basic

environments (Du et al., 2007). In this amperometric enzyme sensor, the H_2O_2 formed by the AOx-AuNPs catalyzed oxidation of alcohol was used as redox indicator to generate the Faradic current response. The fabricated bioelectrode has been characterized and its response characteristics for the substrate ethanol in real samples has been evaluated and presented here.

2. Experimental

2.1. Chemicals and reagents

AOx from *Pichia pastoris* (32 U mg^{-1} protein), horse radish peroxidase (HRP), $HAuCl_4$, chitosan from crab shells (≥75% deacetylated), aniline, uric acid, ascorbic acid, lactic acid, urea, (±)–10–camphorsulfonic acid, 2, 2'-azino-bis [3-ethylbenzothiazoline-6-sulfonic acid] (ABTS), Nafion117 (Nf) (5% w/v in isopropanol) were purchased from Sigma Aldrich. Ethanol, K_2HPO_4, KH_2PO_4 and H_2O_2 (30 % v/v) were purchased from Merck. Chitosan solution (0.2 % w/v) was prepared by dissolving 0.2 g chitosan powder in 100 ml of 1.0 % glacial acetic acid solution. Aniline was purified by passing 1.5 ml of aliquots through a neutral Al_2O_3 column (5 cm long, 0.4 cm diameter) to remove all colored components. All other chemicals were of analytical grade and used as received without purification. AOx (1 mg/ml) and HRP (1 mg/ml) were freshly prepared in 50 mM potassium phosphate buffer solution (KPBS), pH 7.5 and 7.0, respectively.

2.2. Enzyme assay

The AOx activity was measured by HRP-coupled assay method (Kemp et al., 1988). The assay was used to monitor the production of H_2O_2 at $\lambda_{405\ nm}$ for ABTS radical at 25 °C (ε_{405} = 18,400 $\mu M^{-1}\ cm^{-1}$). One unit of enzyme activity was expressed as the amount of enzyme required to produce 1 μM H_2O_2 min^{-1} at 25 °C.

2.3. Characterization methods

Uv-vis spectroscopic measurements were done on a Cary 300 bio (Varian, USA) spectrophotometer with a scan range of λ_{300nm}-$\lambda_{800\ nm}$, using 1 cm path length quartz cuvette at 25 °C. Circular Dichroism (CD) measurements were carried out by using a Jasco J-815 spectropolarimeter calibrated with 0.06 % (w/v) aqueous solution of (±)–10–camphorsulfonic acid. The spectra were recorded at a scan rate of 50 nm min^{-1} in a 0.1 cm path length suprasil quartz cuvette from λ_{190nm} - $\lambda_{240\ nm}$, a bandwidth of 1 nm with 4 accumulations and a time constant of 4 s. The spectra were corrected for baseline and the secondary structure analysis was performed by using DICHROWEB (Whitmore and Wallace, 2008). Transmission electron microscopy (TEM) images are acquired with a 200 kV electron microscope (JEOL JEM, 2100). The Fourier transform infrared spectroscopy (FTIR) measurements were conducted on a Perkin Elmer spectrometer operated at a resolution of 4 cm^{-1}. Dynamic light scattering (DLS) and zeta potential measurements were carried out in a Zetasizer Nano Instrument system (Malvern Instruments Ltd., England). Data were acquired at 20 °C, repeated 20 times and averaged. The viscosity was set to 1 cP at a scattering angle of 90° and resulting autocorrelation function was analyzed by the integrated control software to obtain size and charge distributions. Gel filtration experiments were carried out at RT on a Sephacryl S-300 (10/50) (M_r cut off 500 - 1500 KDa) column using an ACTA FPLC device (GE Healthcare). The column was equilibrated with 3 bed volumes of 50 mM phosphate buffer (pH 7.5). Sedimentation velocity experiments were performed with Beckman optima XL–A/XL–I analytical ultracentrifuge equipped with An50–Ti rotor and the operation conditions were: 82,575 x*g,* 20 °C, Scans at λ_{280nm} and interval of 180 s. Data obtained as absorbance at λ_{280nm} versus cell radius were fitted using continuous sedimentation co-efficient distribution *c(s)* analysis with SEDFIT (Schuck, 2003). AFM was performed using an ambient air scanning probe microscope (Agilent Technologies 5500, USA). Images were recorded with typical contact mode using Picoscan 5 software.

2.4. Preparation of AOx stabilized AuNPs

All glassware were washed with Aqua Regia (HCl: HNO_3, 3:1 v/v), and rinsed with ultrapure water. A total 0.1 ml of aqueous $HAuCl_4$ solution (1 mM) was added to 0.1 ml of AOx solution (1 mg/ml) under shaking at 37 °C. An aliquot of NaOH (1 M, ~5 µL) was then added to the solution after 5 minutes to adjust pH 8.5. The reaction solution was kept in shaking incubator at 37 °C for 24 h for the formation of the AuNPs.

2.5. Preparation of PANI/AOx-AuNPs nanocomposites

A bulk solution consisted of 200 mM aniline, 1 mg/mL AOx stabilized AuNPs and 20 mM ethanol were allowed to stand at 4 °C in dark. The progress of the polymerization of aniline to PANI was evaluated at λ_{450nm} (Supplementary figure 1). PANI was synthesized by oxidative polymerization of aniline using H_2O_2 generated from the AOx catalysed oxidation of alcohol. During this process, cation or cation radical sites generated in monomer (polymer) molecule initiated the polymer growth (Sapurina and Shishov, 2012). After 24 h of reaction time, the solution was centrifuged at 5000xg for 3 min. The precipitated nanocomposites were collected and again transferred into 200 µL of the same buffer and then subjected to 5000xg for 3 min. The washing buffer solution was removed and PANI/AOx-AuNPs particles were collected and stored in 200 µL of KPBS, pH 7.5 for further use.

2.6. Fabrication of bioelectrode

A GCE (diameter 0.5 cm) was cleaned by following a reported method (Das and Goswami, 2013). 100 µL of 0.2 % chitosan was mixed with 200 µL of PANI/AOx-AuNPs and the resulting solution was deposition on a GCE through a step drying process using 3 µL of the solution at a time for 3 times to prepare GCE/chit/PANI/AOx-AuNPs. After complete drying, 5 µL of Nafion (Nf) (5 % v/v) was layered over it and then allowed to dry at RT to produce GCE/Chit/PANI/AOx-AuNP/Nf. Prior to measurements, the surface of the modified

electrodes was thoroughly washed with distilled water. The schematic representation of the fabrication procedure of the AOx-AuNP based bioelectrode is shown in figure 1.

2.7. Amperometric measurements

The electrochemical measurements were done in a three-electrode system containing platinum rod as a counter electrode, Ag/AgCl as reference electrode, and GCE or modified GCE as the working electrode. All potentials were measured and reported relative to the Ag/AgCl reference electrode. Electrochemical Impedance Spectroscopy (EIS) measurements were performed in a background solution of 5 mM $K_3Fe(CN)_6/K_4Fe(CN)_6$ (1:1) and 0.1 M KCl in KPBS within the frequency range of 0.05 Hz to 10 kHz. All experiments were performed at RT.

The amperometric determination of ethanol in commercial samples was performed by the multiple standard addition method. The samples were diluted with KPBS, pH 7.5 in appropriate concentration and passed through 0.22 μM filter disc before analysis.

3. Results and Discussion

3.1. Characterizations of AOx stabilized AuNPs

The Uv-Vis spectra of the solution obtained by mixing AOx with $HAuCl_4$ did not show any characteristic localized surface Plasmon resonance (SPR) peak at λ_{540nm} for AuNPs even after incubating the mixture for several hours (Fig 2A, curve a). The solution however, when adjusted to pH 8.5 with 1 M NaOH and incubated for 6 h at 37 °C, a prominent SPR peak appeared (Fig 2A, curve b). The intensity of the SPR peak was increased with increasing the incubation period of the reaction mixture (Fig 2A, curve c). Above findings demonstrated that AOx protein could initiate the reduction of $AuCl_4$ to the formation of AuNPs under alkaline environment. The TEM images showed the average particle size of 22 nm (in

diameter) with a spread range of 18-24 nm (in diameter) of the enzyme stabilized AuNPs (Fig. 2B). DLS analysis of the reaction mixture incubated for 24 h showed a poly-dispersed particles size in 3 major peaks: the highest intensity at 37± 2.1 nm assigned to the AOx-AuNPs conjugates (Fig. 2 C); the low intensity 10.4 ± 1.5 nm sizes assigned to the unreacted native protein (Supplementary Fig. 4), and peak in the range of 22-26 nm was attributed to the low aggregation of AOx protein. In SEC, the AOx was eluted as single peak with retention time of 21±1.2 min. Whereas AOx and AuNPs mixture (pH 8.5) incubated for 6 h, 12 h and 24 h were eluted as two peaks with retention time of 17.5±0.5 min and 21±0.5 min, respectively (Fig. 2D). The high intensity peak at 17.5±0.5 min corresponds to the AOx-AuNPs and the low intensity peak at 21±0.5 corresponds to the unreacted AOx. The decrease in the retention time implies the formation of AOx-AuNPs conjugates.

The sedimentation coefficients (s) of AOx and AOx-AuNPs (SECpurified) were determined by using a range of "s" values from 15-20 s, and frictional ratio (f/f_0) of 1.2. The fit showed the 's' values of 18.2 ± 0.2 s and 18.6 ± 0.1 s for AOx and AOx-AuNPs incubated for 24 h, respectively (Fig. 2E). Increase in 's' of AOx-AuNPs by 0.3 s indicated the successful formation of AuNPs conjugated AOx. The CD spectra of AOx and AOx-AuNPs conjugate (SEC purified) showed comparable characteristics: a narrow negative peak at $\lambda_{222\ nm}$ and $\lambda_{208\ nm}$, more intense positive peak at $\lambda_{194\ nm}$ with α-helical conformation (Supplementary Fig. 2). A minor difference in the secondary structural composition between AOx and AOx-AuNPs (Supplementary table 1) occurred possibly due to the interaction of the charged gold nanoparticles with the AOx.

FT-IR spectral (Supplementary Fig. 3) analyses of the pure AOx and the AOx-AuNPs pellets shown that the band at 1744 cm^{-1}, which is assigned to the $-COO^-$ of acidic amino acids such as aspartic and glutamic acid residues, was disappeared in AOx-AuNPs implying the potential involvement of $-COO^-$ group of AOx protein in complexing and thus, stabilizing the

AuNPs. A strong band at 2550 cm^{-1} corresponds to the sulphydryl groups (–SH) of cysteine (Aryal et al., 2006) was diminished in AOx-AuNPs indicating involvement of cysteine of AOx protein in reducing $AuCl_4^-$ to AuNPs under alkaline conditions. Additionally a band at 1400-1450 cm^{-1} has been masked in AOx-AuNPs which was assigned to the vibrations of tryptophan residues.

The pH stability of the AuNPs conjugated AOx was studied at pH 3.0 - 11.0 (Fig. 2F) and found the conjugate was less stable at higher acidic (<pH 6.5) and alkaline (>pH 10.0) conditions as the SPR absorbance at these pH conditions decreased with time. The conjugate showed stable absorbance (at λ_{540nm}) at pH 8.5 for 24 hrs. The AOx-AuNPs also showed good stability in NaCl concentration in the range 10^{-5} M to 10^{-1} M (Supplementary Fig. 5). The AOx (p*I* 4.5) showed a zeta potential of -30 mV at pH 7.5. The zeta potential recorded for AOx-AuNPs was -57 mV, implying the possible contribution of negative charge of AuNPs into the conjugate potential (Supplementary Fig. 6).

The Michaelis-Menten constant (K_m) and turnover number (K_{cat}) determined for AOx were 1.92 ± 0.02 mM and 0.165 ± 0.02 s^{-1}, respectively. The K_m and K_{cat} for the AuNPs conjugated AOx were 1.72 ± 0.01 mM and 0.170 ± 0.01 s^{-1}, respectively. Thus, the efficiency (K_{cat}/K_m) of the AOx was increased by 18 % in AOx-AuNPs. There were no significant changes on the kinetic parameters for the AOx when it was merely mixed with the AuNPs prepared by citrate reduction method. The results confirmed the activating role of AuNPs for AOx in the self assembled enzyme-nano conjugate system.

3.2. Characterization of bioelectrode

3.2.1. Morphological characteristics

3D AFM images were recorded to characterize the morphological changes of the electrode surface obtained after each major steps of fabrication. Fig 3A shows the image of the plane

bare GCE. The AuNPs synthesized by citrate reduction method (Frens, 1973; Turkevich et al., 1951) were homogenously distributed over the electrode surface (Fig 3B). The electrode surface with AOx-AuNPs (Fig. 3C) film was transformed to a heterogeneous character with a mixture of globular structure for protein and particle structure similar to AuNPs as in Fig 3 B. When PANI encapsulated AOx (Fig 3 D) and AOx-AuNPs (Fig 3 E) were assembled on the GCE the apparent sizes of the globules were increased further with a clear heterogeneity and protrusions across the whole surface for the later inferring significant increase in electrode surface area relevant for greater immobilization of biomolecules. The diameter of the clusters showed 250 nm and 287 nm for PANI/AOx and PANI/AOx-AuNPs, respectively. The images indicate that the PANI encapsulated AOx-AuNPs nanocomposite was successfully incorporated on the electrode surface. The surface morphology changed to smooth even form when chitosan and nafion were added for the formation of the film in GCE/Chit/PANI/AOx-AuNP/Nf electrode (Fig. 3F).

3.2.2. Electrochemical characteristics

CV of bare GCE and modified GCE was done in an KPBS (50 mM, pH 7.5) at 50 mV s^{-1} to monitor changes in their electrochemical behaviour introduced at different steps of electrode modification. No clear peaks were observed for bare GCE (Fig 4A, curve a) and GCE modified electrodes GCE/Chit/PANI/AOx/Nf and GCE/Chit/PANI/AOx-AuNPs/Nf (Fig 4A, curve b, and c) suggesting that PANI/AOx-AuNPs layer is electro-inactive in this potential window. The addition of ethanol on GCE/Chit/PANI/AOx-AuNPs/Nf bioelectrode however, generated a broad oxidation peak at around +0.6 V (Fig 4A, curve d), which is attributed to the oxidation potential of H_2O_2 (Patel et al., 2001; Xian et al., 2006) formed by the electro-catalytic oxidation of ethanol. The Faradic current at 0.6 V increased with increasing ethanol concentration on the modified electrode (Fig 4A, curve e).

EIS was employed to further monitor the charge properties on the bioelectrode surface during the stepwise assembly of the electrode. The impedance spectra presented as Nyquist plots ($-Z''$ vs Z') obtained on different modified electrodes in a solution of 5 mM $K_3Fe(CN)_6/K_4Fe(CN)_6$ (1:1) and 0.1 M KCl in 50 mM KPBS (Fig 4B). The value of the charge-transfer resistance (R_{ct}) at the electrode surface can be estimated directly from the diameters of the high frequency semicircle. The bare GCE exhibits a line with small semicircle diameter with R_{ct} of 171 Ω (Fig 4B, curve a). The semicircle disappeared upon layering of PANI onto the GCE, implying highly conductive PANI film facilitates the charge transfer with the electrode (Fig 4B, curve b). Reappearance of a semicircle line with R_{ct} of 450 Ω (Fig 4B, curve c) upon layering of PANI/AOx and Nf on the GCE film indicates the successful formation of the film, which increases R_{ct} due to the formation of a ferrocyanide transport-blocking layer on the electrode. The R_{ct} of the GCE was drastically increased to 950 Ω (Fig 4B, curve d) when Chit/PANI/AOx/Nf were layered on it. This implies that the assembled chitosan/Nf layer generated an obstruction to the electron transfer of the electrochemical probe at electrode surface. The R_{ct} of the electrode decreased to 690 Ω when Chit/PANI/AOx-AuNPs/Nf was layered on the electrode surface (Fig 4B, curve e), implying that AuNPs play an important role in accelerating the electron transfer process.

3.3 Application of AOx-AuNP based bioelectrode for sensing ethanol

From a typical current-time plot (Figure 5A) it revealed that the peak current increased linearly (R^2= 0.9731) with increase in ethanol concentrations in the range of 10 µM – 4.7 mM for the bioelectrode GCE/PANI/AOx-AuNPs/Nf (Fig. 5B, curve iii). The limit of detection (DL) and sensitivity of the bioelectrode for ethanol were 7±0.027 µM and 68.3±0.35 µA mM^{-1} cm^{-2}, respectively; where DL = (3 × SD)/sensitivity, and SD (n = 3) is the standard deviation for the points used to construct the calibration curve and the sensitivity, its slope (Supplementary Table 2). The sensitivity and linear range of the GCE/PANI/AOx-AuNPs/Nf

biosensor (Fig 5B, curve iii) was higher than the bioelectrodes that void AuNPs (Fig 5B, curve i and ii). The reason is attributed to the increased loading of ~ 12 % catalytically active AOx on the electrode surface supported by the enhanced immobilization surface area due to the AuNPs. Additionally, the interfacial layer of AuNPs likely to play supporting role in enhancing the kinetics of the enzyme as reported previously (section 3.1) and facilitating the electron hopping from the redox indicator (H_2O_2) to the electrode surface due to its high conductive property. The operational stability of the electrode was investigated for 32 successive measurements with 4.0 mM of alcohol during a period of 5 h. Results demonstrated that the bioelectrode maintained 93.7 % of its initial activity at the end of 25 measurements (Supplementary Fig. 7A). The response of three bioelectrodes prepared by similar procedure to various alcohol concentrations was examined and found acceptable reproducibility with a relative standard deviation (RSD) of ~2.4 % for the response. The storage stability of the bioelectrode was examined by carrying out the response measurements at a regular interval of 3 days and found that the bioelectrode retains ~93 % of the original response even after five weeks when stored at 4 °C and pH 7.5 in 50 mM KPBS (Supplementary Fig. 7B). The half-life ($t_{1/2}$) of the biosensors under the above storage condition was ~302 days. The effect of potential interfering agents present in real samples namely, ascorbic acid, lactic acid, glucose, urea and uric acid, on biosensor response was studied in 50 mM KPBS (pH 7.5) by exposing the sensor separately to these compounds with ethanol in 1:1 ratio. Results showed that these compounds did not significantly affect the biosensor response (Supplementary Fig. 7C) as evident from the selectivity co-efficient (SC) of ~1 for each of the compounds, where $SC = I_{c+i}/I_c$, and I_{c+I} and I_c are response for alcohol in the presence and absence of each interferent, respectively.

The ethanol content (% v/v) in three different beverage samples was determined (at +0.6 V) using the GCE/Chit/PANI/AOx-AuNPs/Nf biosensor and found to be 4.5±0.14, 13.4±0.21

and 52±0.17 % for beer, wine and spirit, respectively. The concentrations of ethanol in the same samples were also measured by gas chromatography and found to be 4.4±0.15, 13.5±0.12 and 51.8±0.2 % for beer, wine and spirit respectively. The comparison of the data was done by paired t-test (Sigma 11) and no significant difference was found (P = 0.709) between the results obtained by the methods. The study validates the reliability of the existing biosensor for sensitive and quantitative analysis of alcohol samples.

A comparative analysis on the performance of various prominent alcohol biosensors reported over the last decade was carried out (Patel et al., 2001; de parda et al., 2003; Hasunuma et al., 2004; Smutok et al., 2006; Tsai et al., 2007; Gouveia-Caridade et al., 2008; Manso et al., 2008; Lee and Tsai, 2009; Das and Goswami, 2013; Jimenez et al., 2014; Soylemez et al., 2014; Chinnadayyala et al., 2014) (Supplementary table 3). The operational and storage stability of the constructed biosensor are comparable to and even improved than many of the reported prominent biosensors. The dynamic detection range of the biosensor was far wider than most of the alcohol biosensors reported so far except an ADH-based biosensor reported recently (Jimenez et al. 2014). However, the lowest detection concentration in the dynamic range obtained by us (0.01 mM) is far lower than the aforesaid ADH-based biosensor (0.9 mM). The ultralow detection limit of the constructed biosensor is considered as beneficial for detecting precisely very low concentration of alcohol in real samples. The overall performance of the biosensor is improved than the previously reported alcohol biosensors. The cause of improved stability and linear range of the present biosensor is ascribed to the amplified activity and high loading of the AOx obtained by its conjugation with activator AuNPs and the highly favorable conformation to AOx provided by the PANI film involved in the fabrication process. The improved kinetic parameter of the AOx-AuNPs had substantially contributed to the aforementioned improved functional activities of the biosensor (Supplementary table 2). The encapsulation of AOx conjugates within enzymatically

synthesized conductive PANI nanoparticles offered a significant storage, operational stability and reproducible response of the biosensor.

4. Conclusions

A stable AOx protein surface stabilized AuNPs synthesized by exploiting the native chemical drive of the protein molecules under alkaline condition was developed for the first time. In this nanoconjugate the intimately associated AuNPs found to enhance the kinetic activity of the AOx enzyme. The AOx-AuNPs conjugates encapsulated with PANI synthesised by exploiting a localized AOx catalysed oxidative reaction, implanted stably on the GCE by using chitosan and Nafion polymers. This nano composite bioelectrode based biosensor showed high operational and storage stability and wide linear current response against ethanol with very a low detection limit. The linear range is thus sufficient for quantitative analyses of alcohol in clinical, forensic and many other practical applications where sensitive detection of alcohol is important. The biosensor was also effectively used for determination of ethanol in commercial beverage samples. The overall performance of the constructed biosensor validates the potential application of the bioelectrode fabrication concept for developing a commercially viable biosensor device.

Acknowledgments:

We acknowledge the financial assistance from Department of Biotechnology, India to carry out this work. The TEM, AFM facility provided by CIF, IITG is duly acknowledged.

References

Aryal, S., Remant, B.KC., Dharmaraj, N., Bhattarai, N., Kim, C.H., Kim, H.Y., 2006, Spectrochem. Acta. Part A 63, 160–163.

Azevedo, A.M., Prazeres, D.M.F., Cabral, J.M.S., Fonseca, L.P., 2005. Biosens. Bioelectron. 21, 235–247.

Bajpai, S.K., Mohan, Y.M., Bajpai, M., Tankhiwale, R., Thomas, V., 2007. J. Nanosci. Nanotechnol. 7, 2994-3010.

Chinnadayyala, S.R., Kakoti, A., Santhosh,M., Goswami, P., 2014. Biosens. Bioelectron. 55, 120–126.

Das, M., Goswami, P., 2013. Bioelectrochem. 89, 19–25.

deParda, G.V.A., Pena, N., Mena, M.L., Reviejo, A.J., Pingarron, J.M., 2003. Biosens. Bioelectron. 18, 1279–1288.

Du, D., Huang, X., Cai, J., Zhang, A., 2007. Biosens. Bioelectron. 23, 285-289.

Frens, G.,1973. Nat. Phys. Sci. 241, 20–22.

Goswami, P., Chinnadayyala, S.S.R., Chakraborty, M., Kumar A.K., Kakoti, A., 2013. Appl. Microbiol. Biotechnol. 97, 4259–4275.

Gouveia-Caridade, C., Pauliukaite, R., Brett, C.M.A., 2008. Electrochim. Acta 53, 6732–6739.

Hasunuma, T., Kuwabata, S., Fukusaki, E., Kobayashi, A., 2004. Anal. Chem. 76, 1500–1506.

Huang, C.F., Yao, G.H., Liang, R.P., Qiu, J.D., 2013. Biosens.Bioelectron.50, 305–310.

Hussain, T.S., Iqbal, M., Mazhar, M., 2009. J. Nanoparticle. Res. 11, 1383–1391.

Jimenez, A., Armada, M.P.G., Losada, J., Villena, C., Alonso, B., Casado, C.M., 2014. Sens. Actuators B. 190, 111–119.

Kemp, G.D., Dickinson, F.M., Ratledge, C., 1988. Appl. Microbiol. Biotechnol. 29, 370–374.

Lee, A.N., Tsai, Y.C., 2009. Sens. Actuators B. 138, 518–523.

Manso, J., Mena, M.L., Yanez-Sedeno, P., Pingarron, J.M., 2008. Electrochimica Acta 53, 4007–4012.

Omidfar, K., Khorsand, F., Azizi, M.D., 2013, Biosens. Bioelectron. 43, 336–347.

Patel, N.G., Meier, S., Cammann, K., Chemnitius G.-C., 2001. Sens. Actuators B. 75, 101–110.

Prakash, S., Chakrabarty, T., Singh, A.K., Shahi, V.K., 2013. Biosens. Bioelectron. 41, 43–53.

Rangnekar, A., Sarma, T.K., Singh, A.K., Deka, J., Ramesh, A., Chattopadhyay, A., 2007. Langmuir. 23, 5700–5706.

Sapurina, I.Y., Shishov, M.A., 2012. Oxidative Polymerization of Aniline: Molecular Synthesis of Polyaniline and the Formation of Supramolecular Structures. In: New Polymers for Special Applications; Gomes, A.D.S., (Ed.), InTech., ch. 9, pp. 251-312.

Sarma, A.K., Vatsyayan, P., Goswami, P., Minteer, S.D., 2009. Biosens. Bioelectron. 24,

Saxena, U., Chakraborty, M., Goswami, P., 2011. Biosens. Bioelectron. 26, 3037–3043.

Saxena, U., Goswami, P., 2012. J. Nanopart. Res. 14, 813.

Schuck, P., 2003. Anal. Biochem. 320, 104–124.

Shankar., S.S., Rai., B., Ahmad, A., Sastry, M., 2005. Chem. Mater. 17, 566–572.

Si, S., Mandal., T.K., 2007. Chem. Eur. J. 13, 3160-3168.

Singh, A.V., Bandagar, B.M., Kasture, M., Prasad, B.LV., Sastry, M., 2005. J. Mater. Chem. 15, 5115–5121.

Smutok, O., Ngounou, B., Pavlishko, H., Gayda, G., Gonchar, M., Schuhmann, W., 2006. Sens. Actuators B. 113, 590–598.

Soylemez, S., Kanik, F.E., Uzun, S.D., Hacioglu, S.O., Toppare, L., 2014. J. Mater. Chem. B. 2, 511-521

Spirin, M.G., Brichkin, S.B., Razumov, V.F., 2005. Colloid J. 67, 485–490.

Syed, M.A., 2014. Biosens. Bioelectron. 51, 391–400.

Tsai, Y-C., Huang, J-D., Chiu, C-C., 2007. Biosens. Bioelectron. 22, 3051–3056.

Turkevich, J., Stevension, P.C., 1951. J. Hiller Disc. Faraday Soc. 11, 55–75.

Wang, J., Musameh, M., Lin, Y., 2003. J. Am. Chem. Soc. 125, 2408–2409.

Whitmore, L., Wallace, B.A., 2008. Biopolymers 89, 392–400.

Xian, Y., Hu, Y., Liu, F., Xian, Y., Wang, H., Jin, L., 2006. Biosens. Bioelectron. 21, 1996–2000.

Zhao, M., Wu, X.M., Cai, C.X., 2009. J. Phys. Chem. C. 113, 4987–4996.

Zhong, Z.Y., Luo, J.Z., Ang, T.P., Highfield, J., Lin, J.Y., Gedanken, A., 2004. J. Phy. Chem. B. 108, 18119–18123.

Figure legends

Figure 1: The schematic representation of the fabrication procedure of AOx-AuNP based bioelectrode.

Figure 2: (A) Uv-vis Spectra: (a) AOx mixed with $HAuCl_4$, pH 7.5 and incubated for 24 h; (b) AOx mixed with $HAuCl_4$ adjust to pH 8.5 with 1 M NaOH and incubated for 6 h and (c) 24 h. Concentration of AOx and $HAuCl_4$ in the analyses was 1 mg/ml and 1 mM, respectively. (B) TEM image of AOx stabilized AuNPs. (C) DLS studies of the reaction solution after 24 h incubation of the AOx with $HAuCl_4$ in KPBS at 20 °C, pH 7.5. (D) SEC of AOx (a) and reaction mixture containing AOx-AuNPs incubated for 6 h (b) 12 h (c) and 24 h (d). (E) Continuous sedimentation co-efficient (*c(s)*) distribution analysis of the simulated data from sedimentation velocity experiment at 4 °C in KPBS showing 's' values for (a) pure AOx and (b) AOx-AuNPs fractions obtained from SEC. The data were fitted using the parameters $\bar{U}$ = 0.73 ml/g and ρ = 1.00 g/cm^3. (F) pH stability studies of the AOx stabilized AuNPs. The different buffers (each of 50 mM) used were sodium acetate (pH 3.5), potassium phosphate (pH 6.5), tris-HCl (pH 8.5) and glycine-NaOH (pH 10.0 and 11.0)

Figure 3: AFM images of GCE (A), GCE/AuNP (B), GCE/AOx-AuNP (C), GCE/PANI/AOx (D), GCE/PANI/AOx-AuNP (E) and GCE/Chit/PANI/AOx-AuNP/Nf (F).

Figure 4: A) CV of GCE (a), GCE/Chit/PANI/AOx/Nf (b), GCE/Chit/PANI/AOx-AuNPs/Nf (c), GCE/Chit/PANI/AOx-AuNPs/Nf with 5 µM (d) and 50 µM (e) ethanol in 50 mM KPBS (pH 7.5) at a scan rate of 50 mV s^{-1}. B) EIS spectra of GCE (a), GCE/PANI (b), GCE/PANI-AOx/Nf (c), GCE/Chit/PANI/AOx/Nf (d) and GCE/Chit/PANI/AOx-AuNPs/Nf (e) electrodes in 5 mM $K_3Fe(CN)_6/K_4Fe(CN)_6$ (1:1) and 0.1 M KCl in 50 mM KPBS.

Figure 5: A) Chronoamperometric current responses of the GCE/AOx/Nf (i), GCE/chit/PANI/AOx/Nf (ii) and GCE/Chit/PANI/AOx-AuNPs/Nf (iii) bioelectrodes at (a) 5 µM (b) 50 µM (c) 500 µM (d) 1.5 mM (e) 3 mM (f) 6 mM successive addition of alcohol. B) Response curves of the bioelectrodes GCE/AOx/Nf (i), GCE/Chit/PANI/AOx/Nf (ii) and GCE/Chit/PANI/AOx-AuNPs/Nf (iii) with increasing ethanol concentration from 5 µM - 6 mM. The operating potential used was +0.6 V (vs. Ag/AgCl electrode).

Highlights

1. A simple method for synthesis of gold nano particles conjugated alcohol oxidase developed.
2. Native chemical drive of the protein under alkaline condition produces the gold nanoparticles.
3. The nano-conjugate showed high and steady stability upto pH 8.5 and NaCl up to10^{-1} M.
4. The efficiency of the enzyme nanoconjugate was increased by 18 % from the free enzyme.
5. Developed bioelectrode using polyaniline encapsulated nanoconjugate with chitosan–Nafion
layer.
6. The overall performance of the biosensor improved than previous reports.

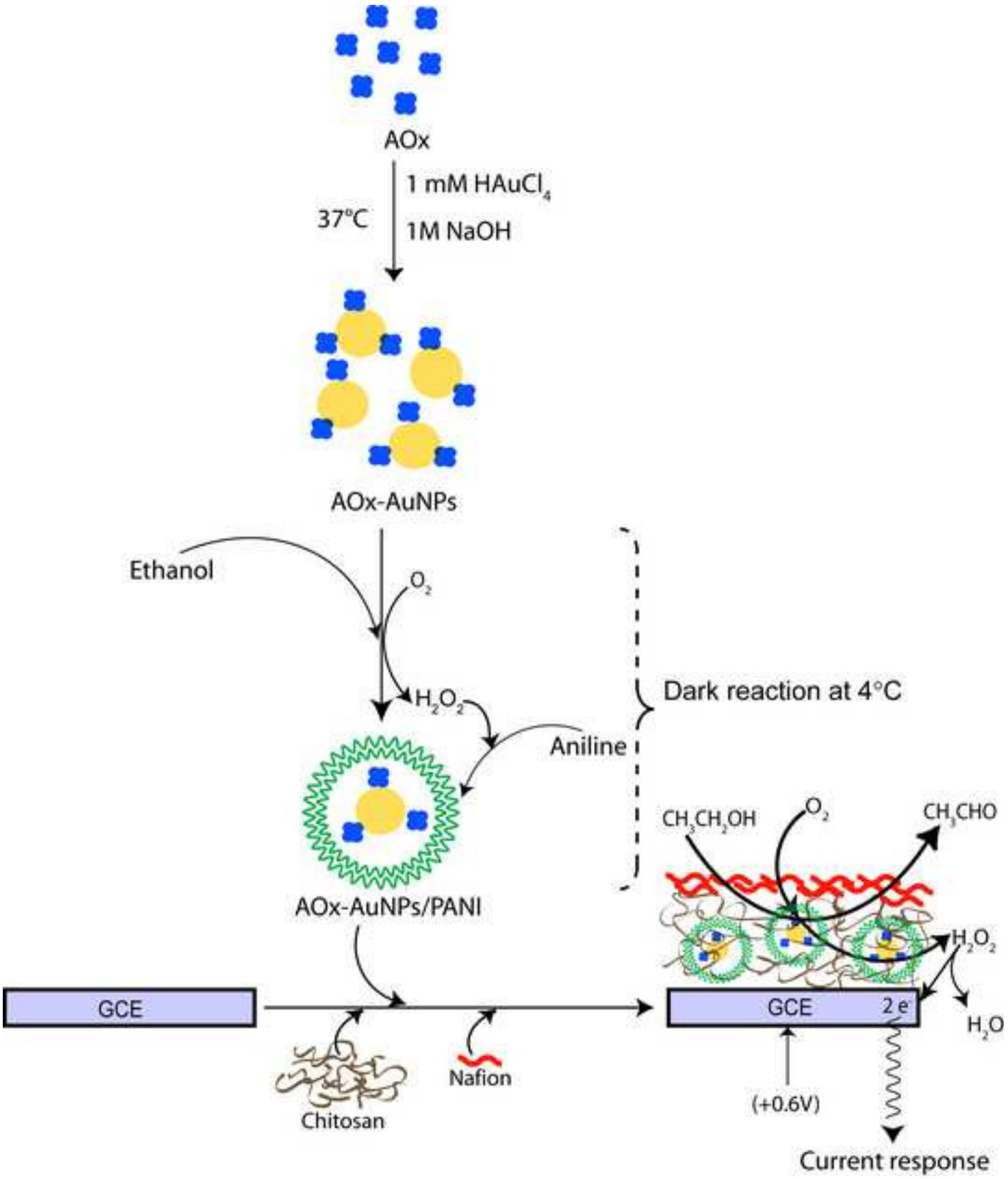

Figure 2

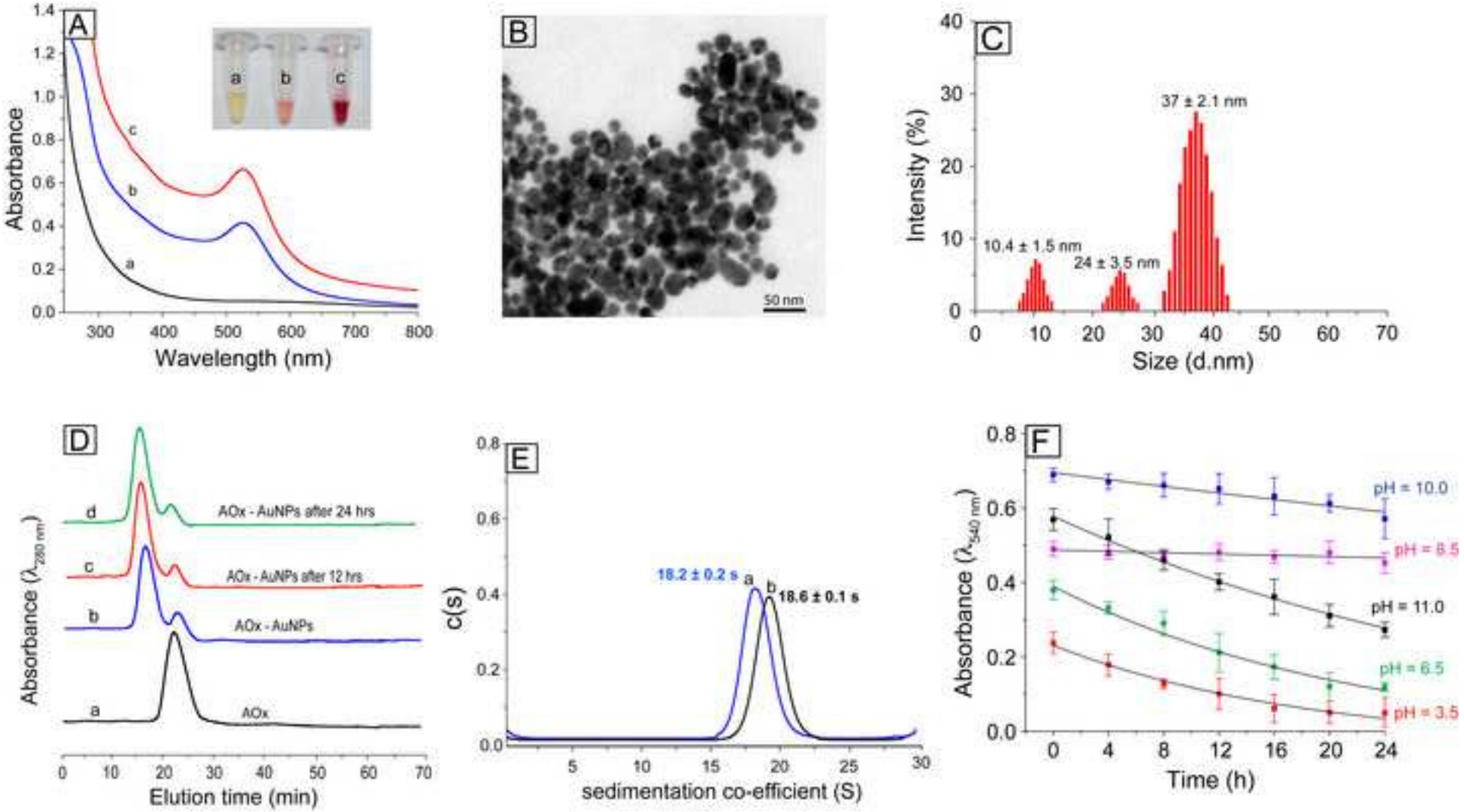

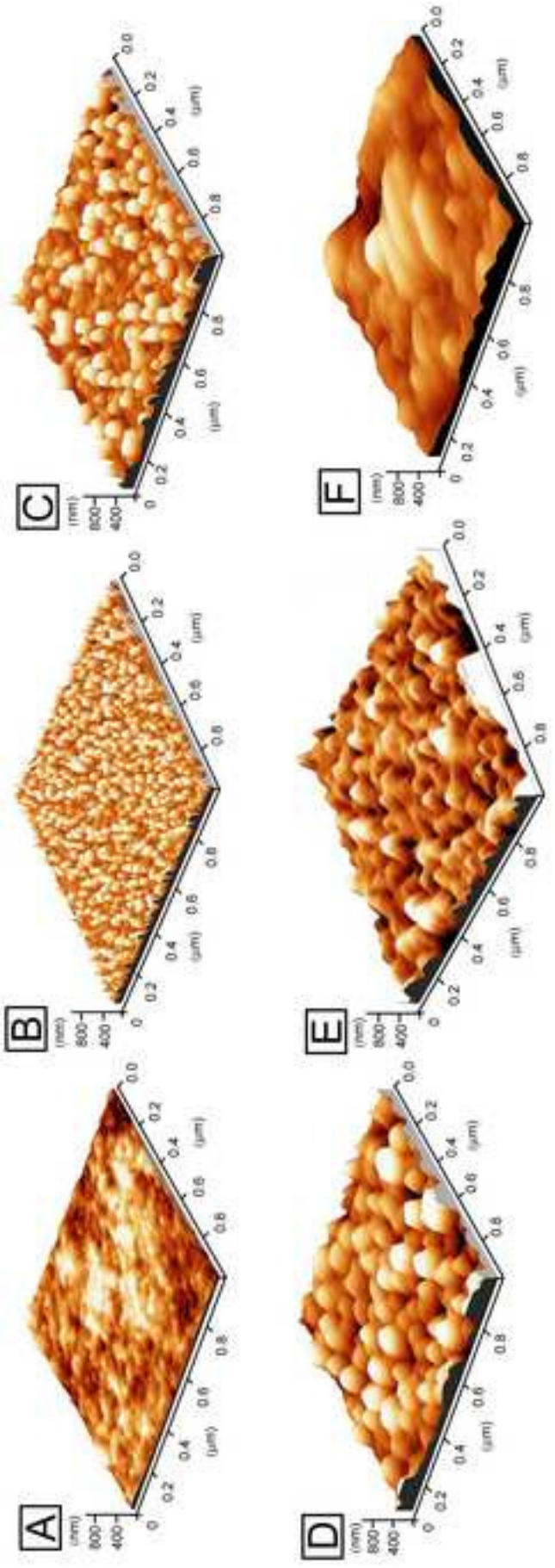

Figure 3

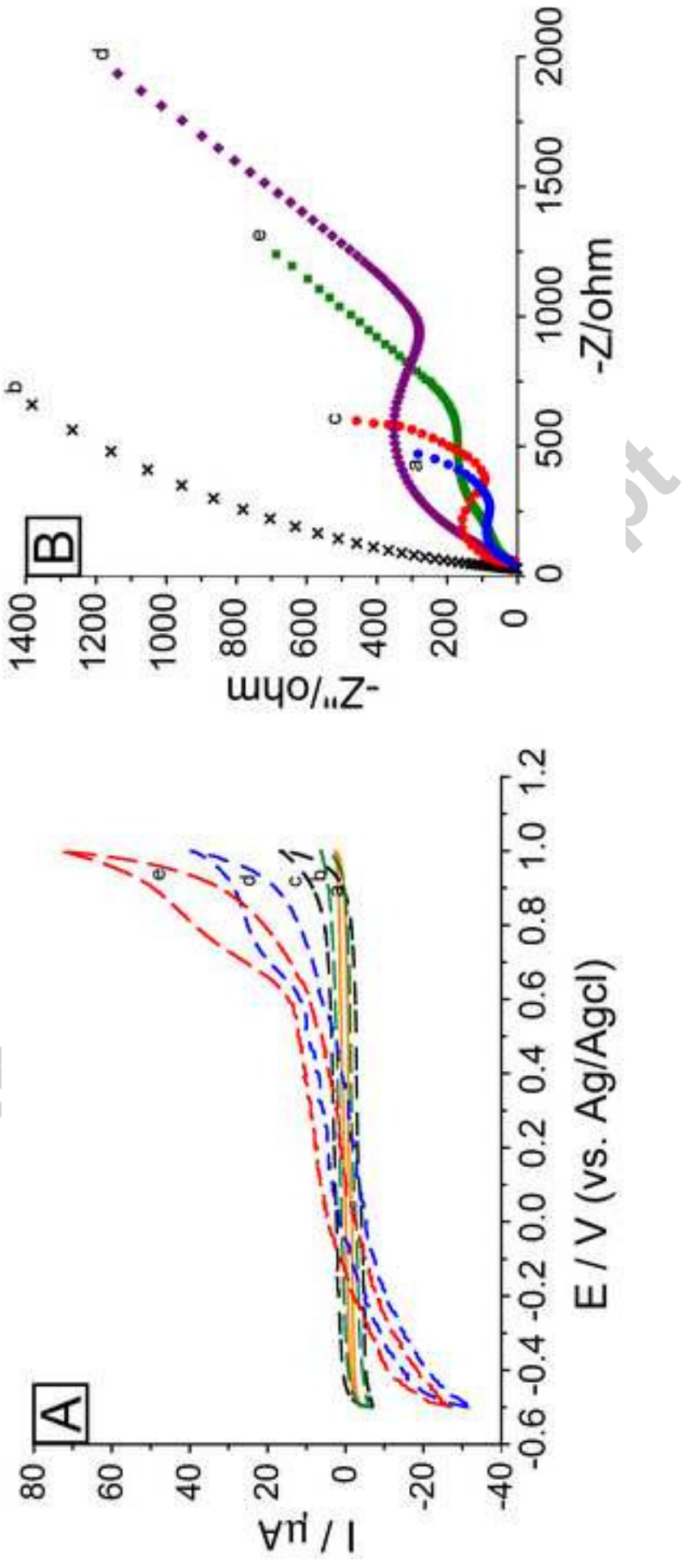

Figure 4

Figure 5